Validation cases for recombining nitrogen and air plasmas

Augustin Tibère-Inglesse, Sean Mcguire, Pierre Mariotto, Christophe Laux

Validation cases for recombining nitrogen and air plasmas

Augustin C. Tibère-Inglesse[1,2], Sean D. McGuire[2], Pierre Mariotto[2] and Christophe O. Laux[2]

[1]*ArianeGroup, 66 Route de Verneuil, 78130 Les Mureaux*
[2]*Laboratoire EM2C, CNRS UPR288, CentraleSupélec, Université Paris-Saclay, 10 rue Joliot-Curie, 91190, Gif-sur-Yvette, France*

We report on Raman scattering and emission spectroscopy measurements in recombining atmospheric pressure plasmas of air and nitrogen. An inductively coupled plasma torch is used to create an equilibrium plasma, which is then forced to rapidly recombine by flowing through a water-cooled tube. For all conditions, temperature measurements are performed using Optical Emission Spectroscopy (OES) and Raman scattering at the exit of tubes of varying lengths. The density of atomic nitrogen is also determined. Evidence of strong chemical nonequilibrium is found in a number of cases. For these cases, we observe that the rotational temperatures measured with OES differ from those measured with Raman scattering, and that the atomic nitrogen density is elevated with respect to equilibrium. A power balance analysis confirms that a large fraction of gas enthalpy is stored in the non-recombined nitrogen atoms. For cases where the plasma remains in equilibrium, we performed numerical simulations using the Eilmer3 CFD code. Eilmer3 does not predict the measured drop in gas temperature measured using Raman and emission spectroscopy. Prior efforts by the CFD community have also failed to correctly predict this temperature drop. The results presented in this paper are therefore intended as validation test-cases for CFD simulations.

I. Introduction

During atmospheric entry, a capsule enters the atmosphere of a planet (Earth, Mars…) at a velocity that can exceed 10 km/s. The strong shockwave that forms in front of the capsule heats the gas to temperatures that can exceed 10,000K. The high temperature of the gas leads to ionization, molecular dissociation, excitation and intense gas radiation. The study of the radiative and convective heat transfer of such a plasma is critical for the design of the heat shield (or thermal protection system, TPS) of the capsule. For high entry velocities, these heatshields are carbon-based and represent a significant constraint for the mission, particularly in regard to their weight. The heat flux to the forebody of the capsule has been the primary focus of past research and is now relatively well understood [1] [2]. However, predictions of the heat flux to the afterbody surface suffer from large uncertainties. This is due mainly to two factors. The first is the presence of significant quantities of carbon in the plasma, introduced via the ablative heat shield in the front of the capsule. The carbon sublimates from the forebody heat shield and recombines in the flow, forming molecules such as CN and CO that emit and absorb radiation in the afterbody region. This is currently the focus of some studies (see for example Refs. [3] [4] [5]). The second phenomenon is the hydrodynamic expansion of the plasma into the afterbody region. This expansion rapidly cools the plasma, forces plasma recombination and a departure from chemical equilibrium. This chemical nonequilibrium and the resulting radiation are not accurately modeled at the moment. Earlier experiments conducted at Stanford University in atmospheric pressure recombining nitrogen plasmas showed that certain transitions emit up to 30 times more than the corresponding equilibrium radiation [6] [7]. CFD simulations were also performed to reproduce the measured atomic N recombination and gas cooling but, as shown in Figure 1, were not in agreement with the measurements [8] [9]. The experiments were conducted with a water-cooled tube mounted at the exit of an atmospheric pressure plasma torch facility. The CFD calculations predicted that the gas temperature decreases by about 400K between the tube entrance and exit for a tube length of 15 cm. These predictions differ dramatically from the measurements, which show a temperature drop of more than 2400K.

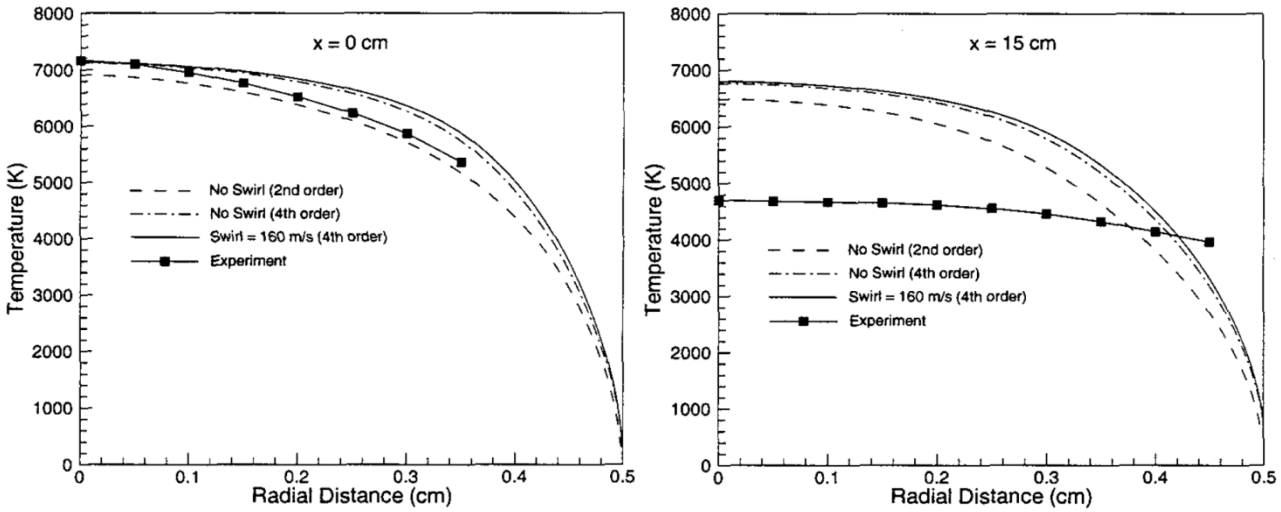

Figure 1: CFD simulations vs experimental results for several CFD simulations. Figures taken from Ref. [9]

The combined effect of these two phenomena, namely the introduction of carbon into the flow and the recombination phenomena, leads to large uncertainties on the heat flux to the afterbody surface. For earth reentry, simulations performed by Johnston *et al* [2] [10] show that uncertainties on the radiative heat flux to the afterbody can be up to 100% for velocities around 14 km/s. The velocity in the case of a real Mars reentry scenario could be higher, particularly for a Mars reentry mission [11] and this would increase the uncertainty resulting from these phenomena.

The heat flux per unit area to the afterbody surface is lower than on the forebody: for example, for the Stardust reentry, the total heat flux on the afterbody is about 20 W/cm² as compared to 100 W/cm² [10] on the forebody. However, the afterbody surface represents approximately 2/3 of the total area, and therefore significant heating may occur on the afterbody. Uncertainties on these afterbody heat fluxes can therefore cause an overestimation of the TPS shield due to design margins. This, in turn, leads to a significant cost increase and added weight.

These considerations can affect the feasibility of a mission. A fundamental study of the mechanisms governing the plasma dynamics in the afterbody of a spacecraft is therefore needed in order to reduce these uncertainties.

In this paper, we revisit the previous experiments conducted by Laux, Gessman *et al* [6] [7] [12] at Stanford University. To that end, we have now implemented a Raman scattering diagnostic to complement emission spectroscopy measurements. Whereas emission spectroscopy gives access to excited states, Raman scattering gives access to the ground state. These techniques are thus complementary. We used our 50-kW plasma torch at the EM2C laboratory to supply a high enthalpy plasma, at conditions reproducing those of the Stanford experiments. The plasma is then cooled in a water-cooled tube to force rapid recombination. If cooling is sufficiently fast, a nonequilibrium plasma is produced at the exit of the tube. We use emission and Raman spectroscopy to study the temperature, chemical composition, and resulting radiation from the plasma. These experiments provide simple test cases of recombining plasmas to validate CFD codes: in particular, they provide validation cases for the chemical kinetics mechanisms used in the CFD codes. We performed experiments for a variety of conditions, ranging from equilibrium to nonequilibrium cases, to assess the impact of the chemical kinetics on the plasma properties.

II. Experimental setup

The plasma torch facility is a TAFA Model 66 inductively coupled plasma (ICP) torch powered by a 120-kVA radio frequency LEPEL Model T-50-3 power supply. The power supply operates at 4 MHz and can supply a maximum of 12 kV DC and 7.5 A to the oscillator plates. Details of the plasma torch facility are provided in previous publications [4] [7] [13]. The plasma produced within the torch exits through a 1-cm diameter nozzle at a speed of approximately 600 m/s. The plasmas studied here are comprised of 90 or 60 slpm of N_2 or air premixed with 50 slpm of argon to provide stable operating conditions for the torch. A water-cooled tube made of brass is mounted on top of the plasma torch. The length of the tube is modular, here up to 25 cm. Emission and Raman measurements are performed at the entrance and exit of the modular tube. Instead of creating a strong expansion as with a reentering capsule, the plasma is forced to recombine by imposing rapid cooling via the cold wall (maintained at approximately 300 K considering the relatively high thermal conductivity of brass). This setup is therefore intended as a simplified experimental model of a real atmospheric entry scenario. Details of the experimental setup are presented in figure 2.

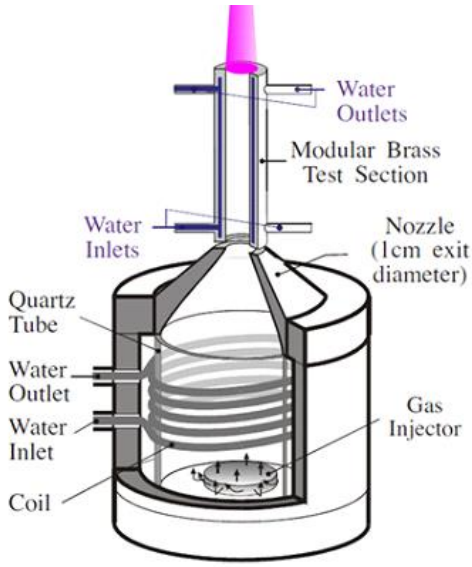

Figure 2: Water-cooled test-section mounted at the exit of the plasma torch

Both Raman scattering and emission spectroscopy measurements were performed for several conditions. Optical emission spectroscopy (see setup in figure 3) is used to measure emission from vibrational bands of the first negative system of N_2^+ and of the first and second positive systems of N_2. When atomic lines are visible, the plasma temperature is measured using absolute emission of several lines of different species, using the procedure detailed in [13]. It is important to note that the use of emission from atomic lines to measure temperature relies on the assumption of equilibrium, which has only been verified to be valid at the entrance of the water-cooled tube and needs to be verified at the exit of the tube. However, where presented, these measurements were found

to be consistent with other measurements of temperature, namely using Raman scattering. If no atomic lines are detectable, the temperature is measured using emission spectroscopy of N_2^+ rotational lines using the procedure detailed in [14]. The measured molecular spectra are compared with theoretical ones generated using the radiation code SPECAIR [15] assuming the measured equilibrium temperature and the known pressure (1 atm). N_2 first positive emission is studied in detail. Here also, the SPECAIR radiation code is used to analyze it. For equilibrium cases, this first positive emission is found to be in good agreement with equilibrium calculations at the measured temperature, providing additional confirmation of the gas temperature for these cases. However, there are a number of cases where the first positive emission cannot be modeled under an assumption of equilibrium. For these cases, a secondary measure of temperature is necessary (e.g. N_2^+ emission or N_2 Raman scattering). It is then possible to adjust the population of all emitting vibrational levels of the N_2 B electronic state in SPECAIR [16] for this transition. This is done using an overpopulation factor for each vibrational level, defined as $\rho_v = \frac{n_v(measured)}{n_v(equilibrium)}$ where n_v is the population density of vibrational level v. The equilibrium value is determined using the temperature obtained via either Raman scattering or N_2^+ emission.

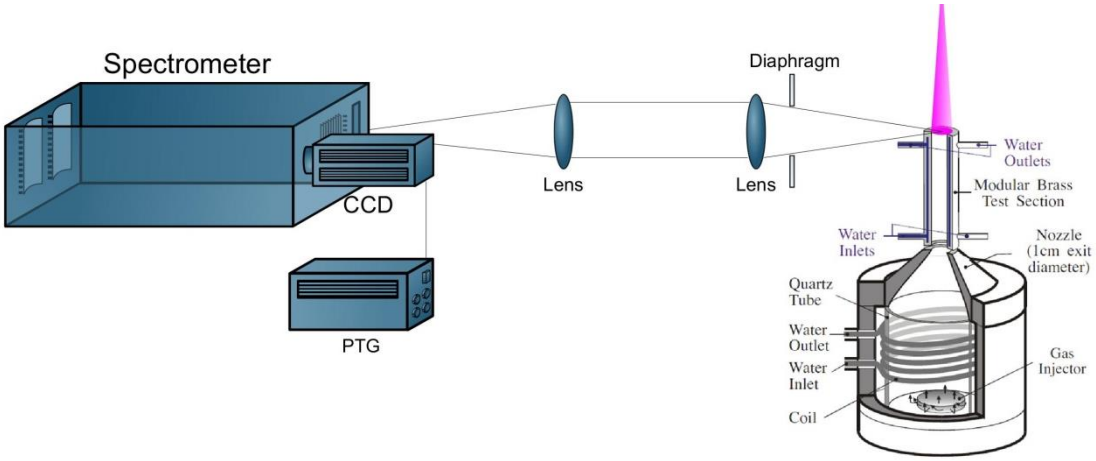

Figure 3: Experimental setup used for emission spectroscopy

All spectra measured using emission spectroscopy are calibrated from pixel counts to absolute emission intensity using an Optronics Laboratories tungsten lamp (model OL550). All spectra are Abel-inverted to obtain the spatially resolved local plasma emission.

To provide an independent confirmation of the gas temperature measured using OES, vibrational Raman scattering measurements have been performed. These yield information on the ground state levels of N_2. Given that the bulk of the gas will be in the ground state, these Raman measurements are more representative of the gas temperature. The experimental setup for Raman spectroscopy is presented in Figure 4 and the detailed measurement procedure is given in Ref [17]. Measurements are performed in the UV region of the spectrum. A frequency-doubled Continuum dye laser was used to generate a 10-ns, 30-mJ ultraviolet pulse at 281 nm. Rhodamine 590 dye was used to form a 562-nm laser beam that was then frequency-doubled to produce the final output beam at 281 nm. While the quadrupled output of a Nd:YAG laser at 266 nm may have sufficed for the measurements, the ability to tune the dye laser offered the ability to avoid potential laser-induced interferences in the UV. The wavelength used for these measurements, namely 281 nm, represents a tradeoff between avoiding laser-induced interferences and maximizing laser power. This Raman technique is sensitive to both the rotational and vibrational temperatures of the N_2 ground state. The results suggest that both temperatures are in equilibrium, so only one temperature will be given in the results section. Moreover, rotational relaxation at atmospheric pressure is very fast and so we assume that rotational and translational temperatures are equal. Additional Rayleigh scattering measurements of density support this assumption [17].

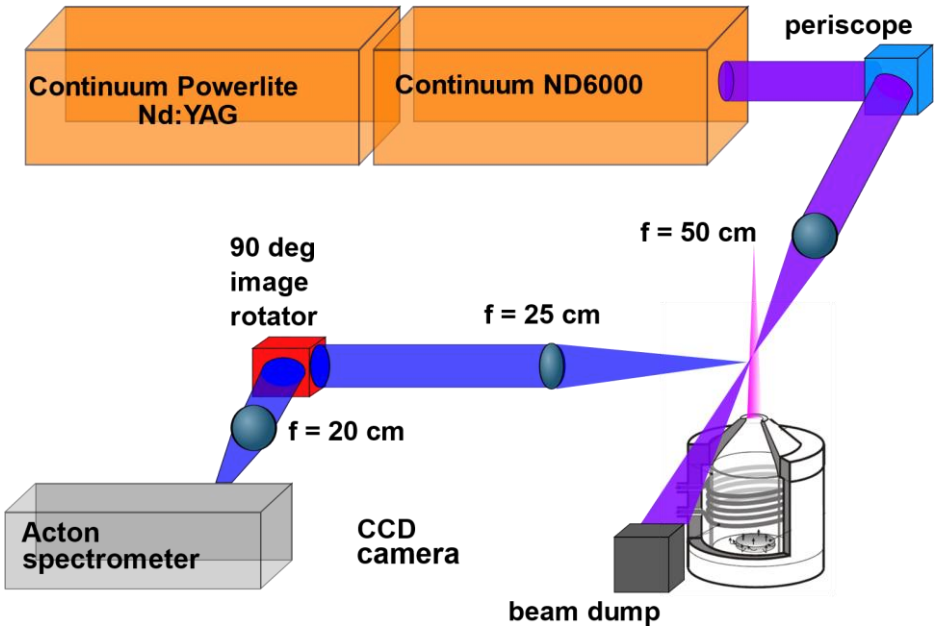

Figure 4: Experimental setup for Raman UV scattering measurements. A periscope consisting of two quartz prisms allows to adjust the height and direction of the laser beam. The 90° image rotator serves to horizontally align the laser beam with the spectrometer entrance slit.

Ultimately, the fluid dynamics and plasma kinetics within the water-cooled tube are coupled. However, in an effort to decouple these effects, experiments were performed for a variety of conditions presented in Table 1. The conditions range from laminar to turbulent regimes and from chemical equilibrium to nonequilibrium. The chemical conditions (equilibrium or nonequilibrium) are estimated based on the results of Gessman et al. [18] and will be verified in the Results section. Note that the measurements for the case 'Pure air' are taken from the paper by Gessman et al [18]. We repeated these experiments and obtained the same results, which are therefore not presented here. For all other cases, the reported results are from the measurements presented in this paper.

	Mass flow rate	Estimated Reynolds number based on the tube diameter	Chemical conditions
Pure air	$\dot{m}_{Air} = 1.9$ g/s	~1900 (laminar)	Equilibrium
Air/Ar	$\dot{m}_{Air} = 1.9$ g/s $\dot{m}_{Ar} = 1.5$ g/s	~3600 (turbulent)	Equilibrium
N_2/Ar 1	$\dot{m}_{N_2} = 1.2$ g/s $\dot{m}_{Ar} = 1.5$ g/s	~2700 (slightly turbulent)	Nonequilibrium
N_2/Ar 2	$\dot{m}_{N_2} = 1.9$ g/s $\dot{m}_{Ar} = 1.5$ g/s	~3600 (turbulent)	Nonequilibrium

Table 1: Measured mass flow rates and expected conditions for the different plasma cases studied. The plasma torch cannot be operated with pure N_2 and thus the N_2/Ar mixture is necessary for studying nitrogen kinetics. The Air/Ar mixture was chosen for comparison with the N_2/Ar 2 case, keeping the same mass flow rate, hence aerodynamic regime, in order to isolate the effects related to chemical kinetics. Note that the turbulent energy of the flow was not measured. The labels 'laminar' and 'turbulent' are based on the Reynolds number estimates.

In the first part of this article, we give an overview of the experiments performed in air/argon or nitrogen/argon mixtures. For each test condition, we provide the temperature profiles measured using both emission and Raman spectroscopy, the emission spectra of the nitrogen first positive system, and the power balance. While the Air/Ar mixture remains in equilibrium, the N_2/Ar mixture is found to be in chemical nonequilibrium at the exit of the tube. For equilibrium cases using the Air/Ar mixture, the underlying dynamics are governed primarily by the

flow regime. Both laminar and turbulent cases are examined. For nonequilibrium cases using the N_2/Ar mixture, both hydrodynamics and chemical kinetic effects are important. The nonequilibrium vibrational distributions within the N_2B electronic state were measured and used to infer the density of unrecombined atomic nitrogen [7]. In the second part of this paper, we will discuss simulations done using the CFD code Eilmer3 [19].

II) Experimental study of Air/Ar and N_2/Ar plasmas

a. Air/Ar

The basic operating conditions for these test cases are presented in Table 1. The gas is air (1.9 g/s) mixed with argon (1.5 g/s). Three tube lengths were investigated: 0 cm (inlet of the tube), 10 and 15 cm. The radial temperature profiles were measured with both Raman scattering and OES. As can be seen in Fig. 5, the two methods are in agreement. For the emission spectroscopy measurements, several atomic lines (Argon at 738, 750, 751 and 763 nm, Nitrogen at 742, 744, 746 nm) were used, and all yielded the same temperature within experimental uncertainty. Therefore, only the temperature profile obtained from the oxygen triplet at 777 nm is presented in the figure. The relatively high uncertainty bars for the Raman measurements at 0 cm are due to the low signal-to-noise ratio, because of the low densities associated with high temperatures, and because nitrogen is highly dissociated at these temperatures. Finally, note that the Raman scattering measurements give both the rotational and vibrational temperatures of N_2 ground state. Because the rotational and vibrational temperatures were found to be equal, only one temperature is presented here.

Overall, the Raman and emission spectroscopy closely match, which indicates that the flow remains close to LTE at all positions. The centerline temperature drop is about 2400 K.

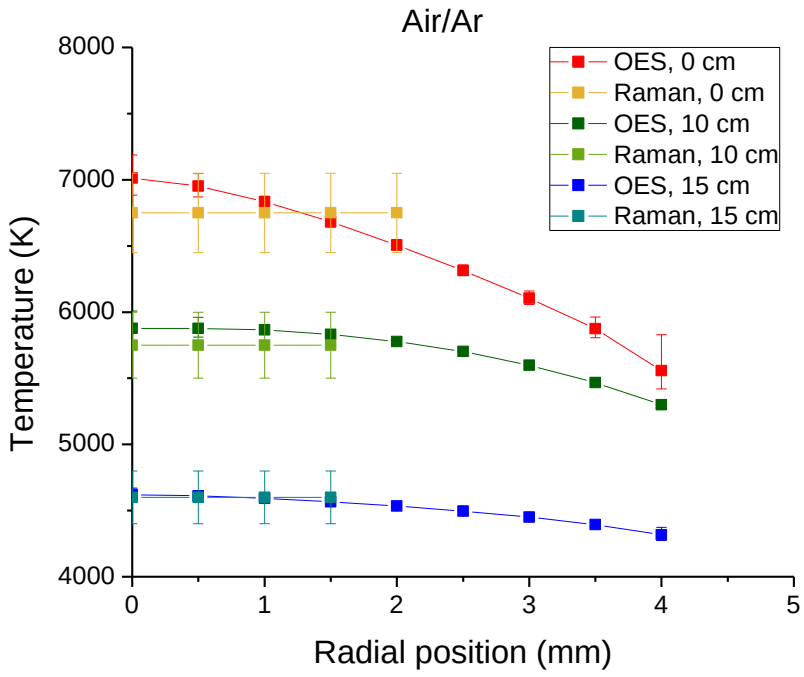

Figure 5: Temperature profiles measured with Raman scattering and OES at 0, 10 and 15 cm for the Air/Ar plasma.

Emission spectra of the N_2 first positive transition were recorded between 550 to 800 nm. These spectra are also calibrated in absolute intensity and are Abel-inverted to produce local volumetric emission. In Figure 6, we compare the Abel-inverted spectrum at the plasma centerline (r = 0 cm) and exit of the 15 cm tube, with the spectrum computed with SPECAIR, assuming equilibrium at the centerline temperature presented in Figure 5 (4660 K).

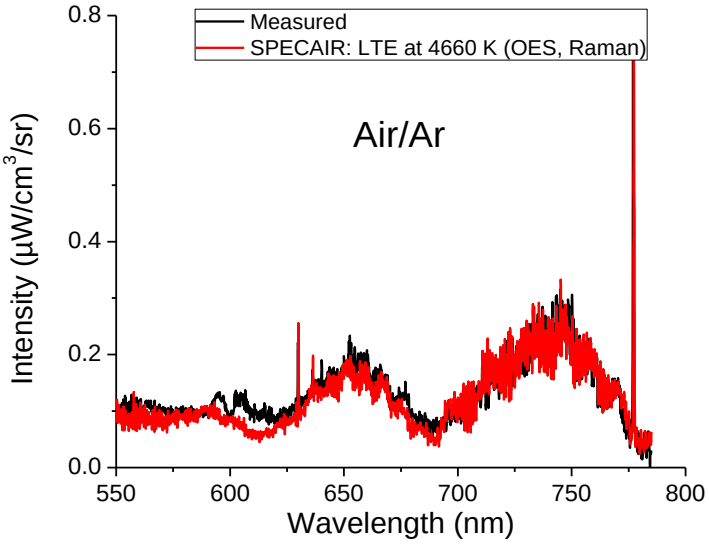

Figure 6: Comparison between centerline experimental and computed spectra at the 15 cm-tube exit. The black curve represents the calibrated Abel-inverted measured spectrum and the red one the spectrum computed with SPECAIR assuming equilibrium at the temperature measured with Raman and emission spectroscopy.

The spectra are in good agreement with one another, with the exception of a small discrepancy between 600 and 625 nm. This agreement confirms the assumption of equilibrium. Similar results are observed for all Abel-inverted spectra at other radial positions, both at the exit of the 10 and 15 cm test-sections.

In addition to the emission and Raman measurements, we also performed a power balance. For this, the difference in water temperature at the inlet and outlet of the tube was measured. The gas enthalpy was also estimated from the measured temperature profiles at the inlet and outlet of the tube. The power balance, assuming equilibrium conditions, is then:

$$\Delta P_{gas\ (equilibrium)} = \left[\int_{r=0\ mm}^{r=5\ mm} \rho_{gas} V_{gas} h_{gas} 2\pi r dr\right]_{outlet} - \left[\int_{r=0\ mm}^{r=5\ mm} \rho_{gas} V_{gas} h_{gas}\ 2\pi r dr\right]_{inlet}$$

where V_{gas} represents the gas velocity, ρ_{gas} the mass density, and h_{gas} the specific enthalpy. The thermodynamic properties of the plasma were calculated using the CEA code [20] at the measured temperatures. Note that the velocity is estimated by matching the mass flow rate and assuming a radial velocity profile self-similar to that of the measured temperature: this is justified by the fact that the Prandtl number is close to unity. The uncertainty on the velocity determined with this procedure is estimated to be 30%.

The calorimetric power balance on the water that traverses the water-cooled tube gives the power removed at the wall and is equal to:

$$\Delta P_{water} = \dot{m}_{water}\ c_{p_{water}} (T_{wo} - T_{wi})$$

where $\dot{m}_{water}$ is the measured water mass flow rate, and T_{wi} and T_{wo} are the temperatures of the water at the inlet and the outlet of the cooling tube, respectively.

Assuming equilibrium conditions for the plasma, the power balance reads:

$$\Delta P_{water} = \Delta P_{gas\ (equilibrium)}$$

The results for ΔP_{water} and $\Delta P_{gas\ (equilibrium)}$ are presented in figure 7.

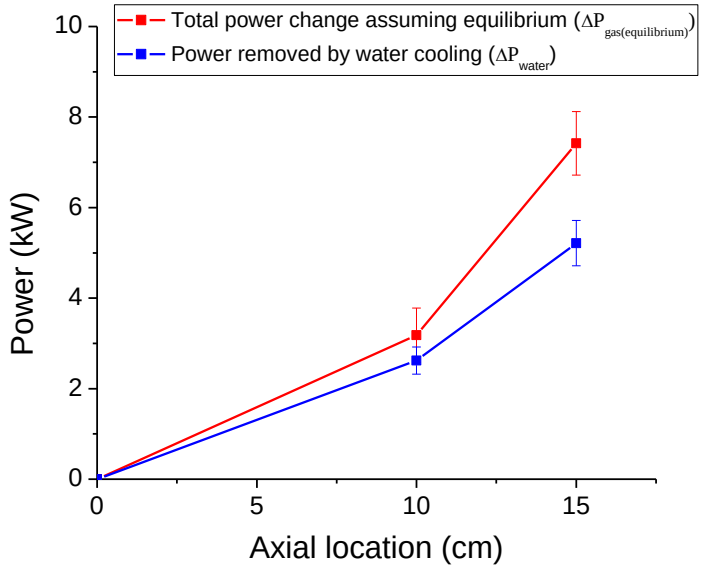

Figure 7: Power measurements using two different approaches. Blue: measured power removed by water cooling. Red: Power change between the exit and the inlet of the tube assuming equilibrium throughout the tube.

At 10 cm, both approaches give the same results to within their respective uncertainty. This supplies additional evidence for the equilibrium assumption. At 15 cm we see a difference between the two lines which may be indicative of a departure from equilibrium. A suspected reason for this discrepancy is an overpopulation of atomic nitrogen near the wall. This is observed to be a very strong effect in the N_2/Ar experiments (presented in section II.b). Unrecombined atomic N can account for a large amount of enthalpy. This hypothesis will be investigated more in the following nitrogen cases. Nonetheless, the relatively good agreement between the two curves here gives us confidence in the fact that the plasma is at least close to equilibrium. Also, this equilibrium case serves as a validation of our Raman measurements because both the Raman and emission spectroscopy measurements are in agreement with one another. Finally, note that we estimated the radiative losses using SPECAIR through the tube outlet and found them negligible (< 10W).

b. N_2/Ar: low mass flow rate

For this case, 1.2 g/s of nitrogen and 1.5 g/s of Argon were injected into the plasma torch. Three axial positions were studied: 0, 10 and 15 cm. Radial temperature profiles were measured at these three locations using Raman and emission spectroscopy. At 0 and 10 cm, the temperature measured using OES was obtained from the absolute intensity of five atomic lines, namely the nitrogen lines at 742, 744 and 746 nm and the argon lines at 751 and 763 nm. All five lines give similar results and therefore only one will be presented (nitrogen at 746 nm here). The temperature at 15 cm is measured using OES of N_2^+ rotational lines as no atomic lines were visible. Note that at 0 and 10 cm, therefore, the temperature measured using OES corresponds to the electronic temperature of atomic species whereas, at 15 cm, it corresponds to the rotational temperature of N_2^+B. For the Raman measurements, the rotational and vibrational temperatures were found to be equal and, therefore, we only give one temperature here. Results are shown in figure 8. At 0 and 10 cm, the temperature measured with both Raman and emission spectroscopy are in agreement with another. At 15 cm, the temperature measured with Raman is slightly lower than the temperature measured with emission spectroscopy.

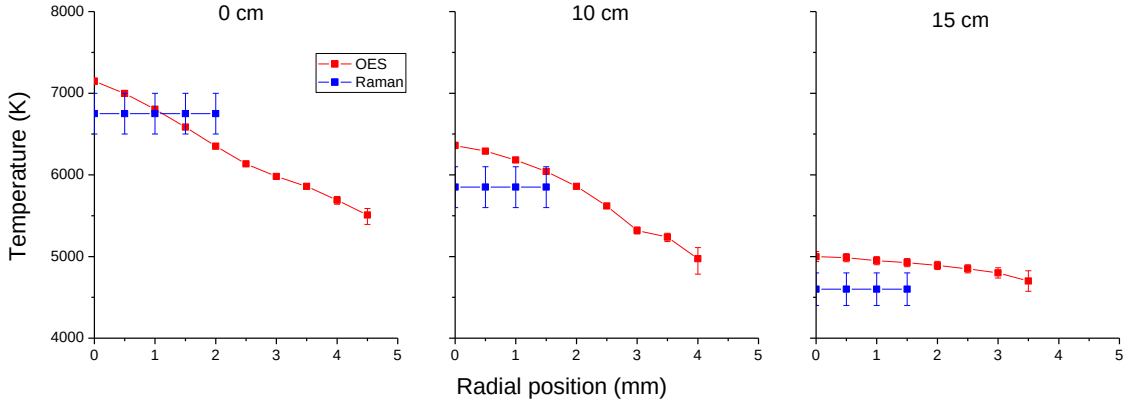

Figure 8: Temperature profiles measured with Raman and emission spectroscopy at 0, 10 and 15 cm for the N_2/Ar plasma at low mass flowrate. The red line represents the temperature measured using emission spectroscopy and the blue one the temperature measured using Raman spectroscopy

At the exit of the 15-cm tube, we also measured N_2 first positive emission between 500 and 800 nm. We compared the measured spectrum with spectra computed using SPECAIR, using the temperatures measured with Raman and emission spectroscopy. Results are shown in figure 9. All measured spectra are Abel-inverted and we present here the centerline spectra.

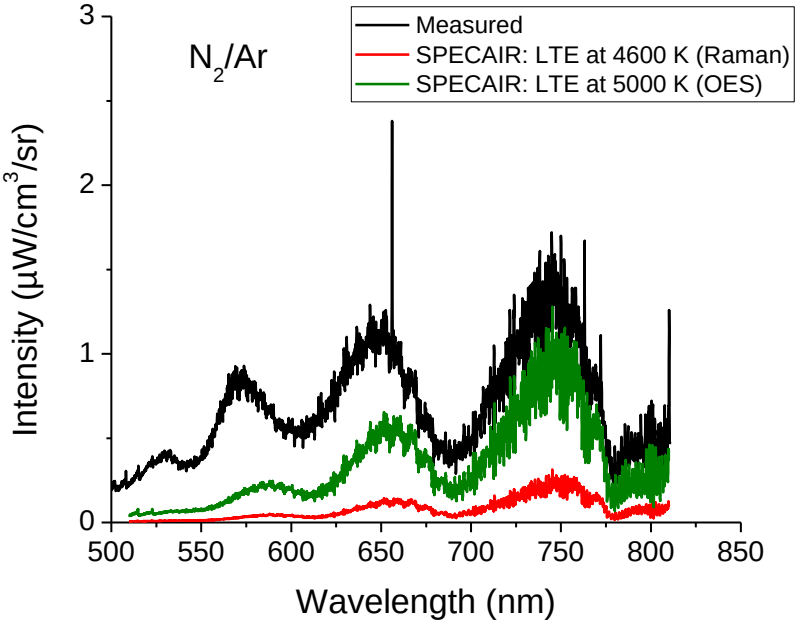

Figure 9: Comparison between the measured spectrum and SPECAIR LTE computations at the temperatures measured with Raman spectroscopy (red line) and with emission spectroscopy (green line) at 15 cm for the N_2/Ar plasma at low mass flowrate.

It is clear from figure 9 that the measured spectrum is very different from the spectra computed assuming LTE at the temperatures obtained from emission spectroscopy (T = 5000 K) and Raman spectroscopy (T = 4600 K). These differences indicate that the plasma is not in equilibrium. We also note that the measured total radiated power between 550 and 800 nm is twice higher than the radiation predicted assuming LTE at the temperature measured via emission spectroscopy, and 10 times higher if we consider LTE at the temperature measured using Raman spectroscopy.

To quantify the degree of departure from equilibrium within the vibrational levels of the N_2 B state, we used the radiation code SPECAIR and altered the population of the individual vibrational levels of N_2B in order to reproduce the experimental spectrum. The experimental spectrum was reconstructed by introducing overpopulation factors for the various contributing vibrational levels and using an optimization algorithm to minimize the difference between computed and experimental spectra. The results of the measured population distribution and the corresponding spectra are presented in figure 10. Here, the rotational temperature is assumed to be the temperature measured using Raman scattering, which is likely to be more representative of the gas temperature.

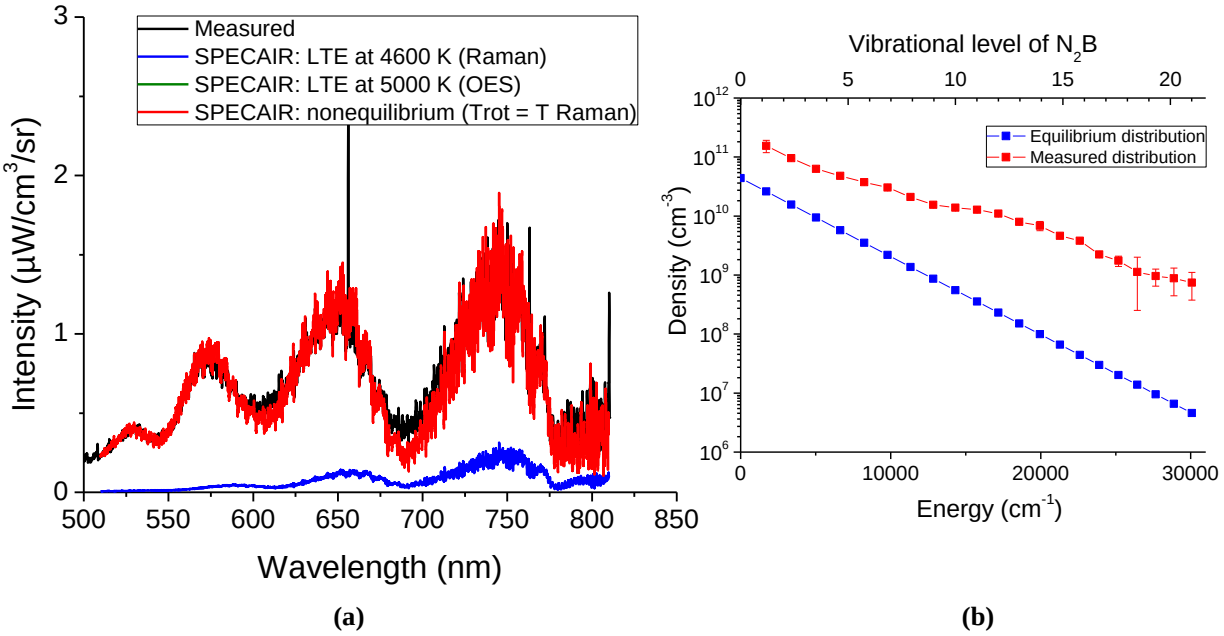

Figure 10. (a) Measured and computed spectra at the exit of the 15-cm tube for the N_2/Ar case at low mass flowrate. (b) Vibrational population distribution of N_2B taken for SPECAIR nonequilibrium calculations.

The good agreement between the spectrum computed using SPECAIR (assuming the nonequilibrium vibrational population distribution shown in Figure 10b) and the experimental one gives us confidence in our measurements of the N_2B vibrational level overpopulation factors. Note that the distribution of vibrational levels of N_2B does not follow a Boltzmann distribution: such a distribution would correspond to a straight line in Figure 10b. It is therefore not possible to characterize this distribution using a single temperature. Furthermore, the total density of all vibrational levels, which yields the density in the N_2B state electronic state, is highly overpopulated with respect to its equilibrium value. To reproduce this overpopulation in CFD simulations, a vibrationally specific model must be used.

This same procedure was repeated to determine the temperature profiles and vibrational distributions in the N_2B electronic state at all radial positions. Figure 10 presents these results at the center location (r=0 mm). Figure 11 shows results at other radial locations. For these, we used the temperature obtained by Raman scattering. The population of the N_2B vibrational levels remains relatively constant over the first 2 mm radius at the exit of the 15-cm tube. This is consistent with the relatively flat temperature profile for a tube length of 15 cm over the same range (Figure 8). This result suggests that a 1D numerical model may be sufficient for reproducing these population distributions.

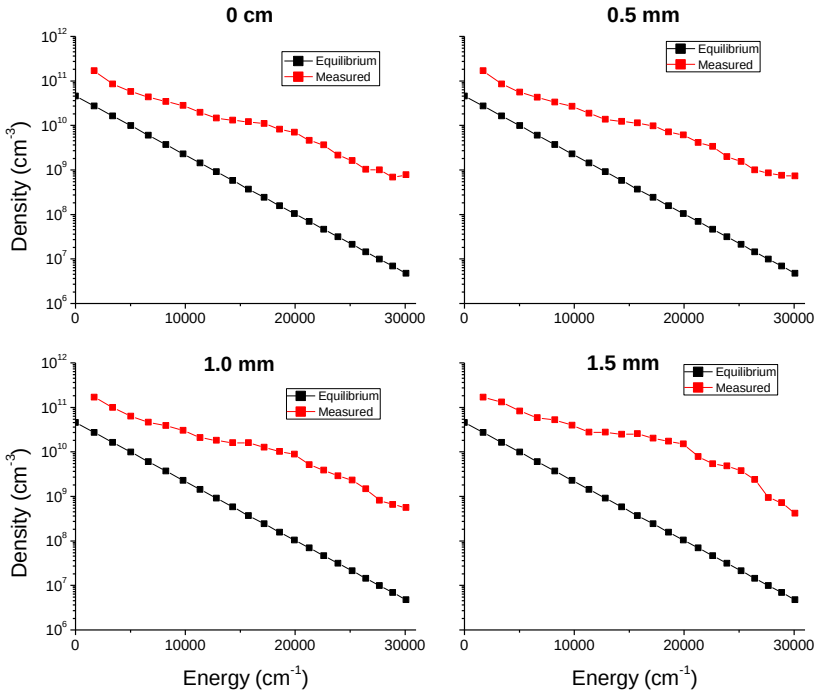

Figure 11: Radial profiles of the absolute density of vibrational levels of N_2B at the exit of the 15-cm tube. N_2/Ar plasma at low mass flowrate.

From these data, it is possible to determine the atomic nitrogen density as a function of radial position as shown in Figure 12. The theory beyond this analysis is explained in Ref. [7]: the vibrational level v=13 of N_2 B is a spontaneously predissociating state, in partial local thermodynamic equilibrium with ground state nitrogen atoms (N^4S):

$$N_2(B, v = 13) \leftrightarrow N(\,^4S) + N(\,^4S)$$

The overpopulation of atomic nitrogen can then be expressed as a function of the measured overpopulation, $\rho_{N_2,B,v=13}$, of vibrational level v=13 of N_2B, via the following equation:

$$\rho_N = \sqrt{\rho_{N_2,B,v=13}}$$

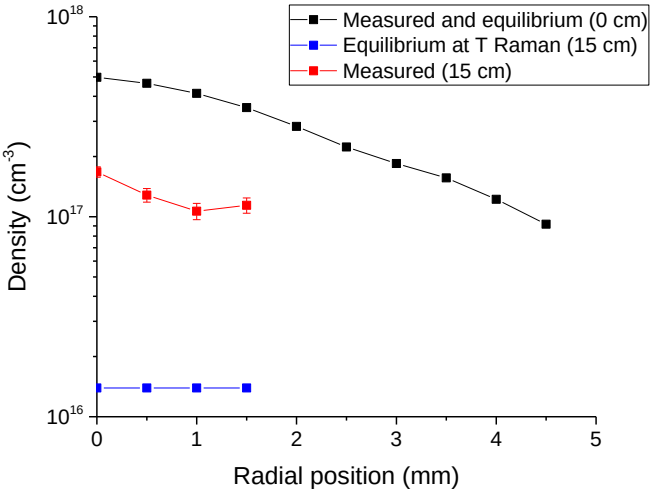

Figure 12: radial population distribution of atomic nitrogen atoms at 0 and 15 cm, measured and calculated assuming LTE at the temperature measured using Raman spectroscopy. N_2/Ar plasma at low mass flowrate.

The measured atomic nitrogen density is well above its equilibrium value at 15 cm. This suggests that atomic nitrogen is partly frozen in the tube. Furthermore, a significant amount of enthalpy is stored in the unrecombined N. This is an important consideration for the power balance. Considering the density measured in figure 12, the enthalpy stored in unrecombined nitrogen atoms is given by the following relation:

$$\Delta H_{chem} = (n_N - n_N^*) E_{diss_{N_2}}$$

where n_N is the measured number density of N, n_N^* is the equilibrium density of N, and $E_{diss_{N_2}}$ the energy of dissociation of N_2. This enthalpy must then be divided by the residence time of the gas in the tube to obtain a power:

$$\Delta P_{chem} = \int_{r=0}^{r=R} \frac{\Delta H_{chem}}{\tau_{\text{residence}}} dr = \int_{r=0}^{r=R} \frac{\Delta H_{chem}}{\frac{x}{V_{gas}(x,r)}} dr$$

where x is the length of the tube (10 or 15 cm) and V_{gas} represents the mean velocity of the gas at the axial position x. Note that the velocity has not been measured directly and is therefore estimated as discussed in Section IIa.

The power balance presented in IIa now becomes:

$$\Delta P_{water} = \Delta P_{gas\,(equilibrium)} - \Delta P_{chemistry}$$

where $\Delta P_{chemistry}$ represents the power stored in chemical and internal modes. We find that the dominant part of this power is contained in unrecombined atomic N. The chemical energy stored in the overpopulated vibrational levels of N_2 B and N_2 C, measured using emission spectroscopy, was also considered but was found to be negligible in comparison. Figure 13 shows the results obtained for the power measurements.

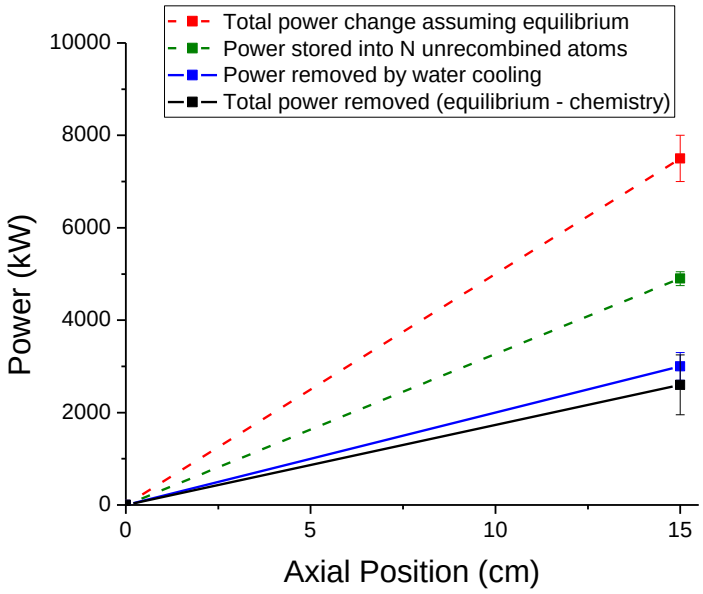

Figure 13: Power balance measurements for the N_2/Ar plasma (low mass flowrate), using two different approaches.
Blue: measured power removed by water cooling.
Red: Power change between the outlet and the inlet of the tube assuming equilibrium throughout the tube.
Green: power stored into unrecombined N atoms using the measured overpopulation factors.
Black (red minus green curve): total power removed from the gas.

For the N_2/Ar plasma, the good agreement between the black and the blue curves suggests that the unrecombined N accounts for the missing energy. This energy balance gives us confidence in our temperature measurements. It also shows the importance of accounting for chemical nonequilibrium in the power balance. Evidently, this

chemical effect is as important as the heat transfer to the water-cooled tube walls. An accurate kinetic model is therefore mandatory to correctly predict the drop in temperature using a CFD code.

c. N_2/Ar: high mass flow rate

For this case we have reproduced the condition of Gessman *et al* [12]. 1.9 g/s of nitrogen was mixed with 1.5 g/s of argon. The mass flow rates are equal to those presented in section IIb for the Air/Ar plasma: air injection was simply replaced with nitrogen injection. The plasma was studied at 0, 10 and 15 cm. Figure 14 shows the radial temperature profiles measured using both Raman and emission spectroscopy.

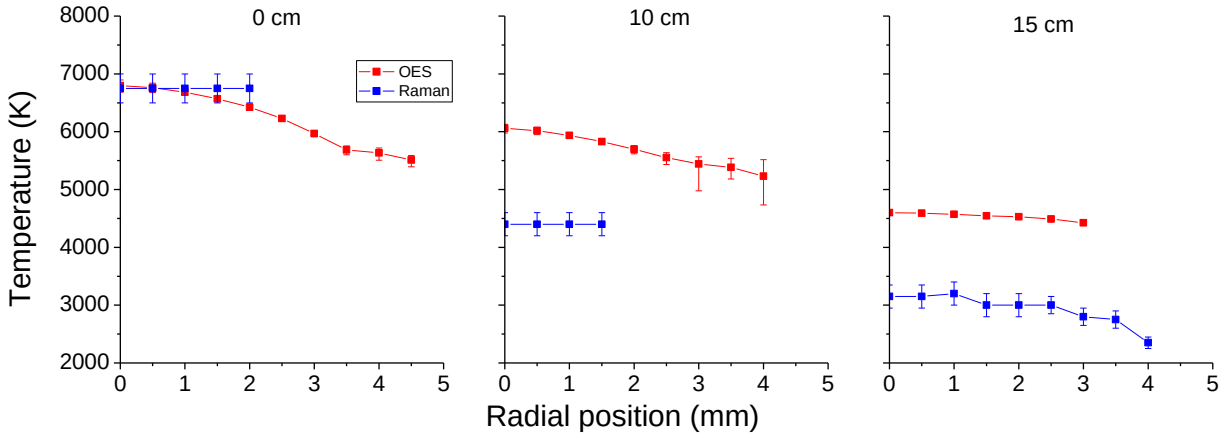

Figure 14: Temperature profiles measured using both Raman and emission spectroscopy at 0, 10 and 15 cm. N_2/Ar plasma at high mass flowrate.

At 0 cm, both Raman and emission spectroscopy give the same temperature measurement. However, at 10 and 15 cm, the temperature measured using Raman scattering is significantly lower than the temperature measured using emission spectroscopy. This was observed to a lesser extent in the previous case (nitrogen/argon at low mass flowrate). Recall that the temperatures measured using OES and Raman scattering were in good agreement for the Air/Ar case. This previous agreement gives us confidence in the temperatures presented here and implies that the difference is not an artifact of the measurement. This difference between the two measurements therefore implies a strong nonequilibrium between the temperature of excited states of nitrogen and the temperature of the ground state. At 15 cm, the temperature measured by emission spectroscopy corresponds to the rotational temperature of the N_2^+ B state. This discrepancy will be discussed at the end of this section.

These observations suggest that our emission measurements may not provide a representative estimate of the bulk gas temperature. The Raman measurements show that the bulk gas temperature is much lower. Referring back to Figure 1, we find that the temperature decrease in the the 15-cm tube is more pronounced than in the experiments of Gessman *et al.* [12]. Furthermore, the measured temperature decrease is much larger than what is predicted by the CFD codes for this high flowrate nitrogen/argon plasma.

As before, we measured the N_2 first positive emission spectrum between 500 and 800 nm at 15 cm, and we compared it with LTE spectra computed with SPECAIR at the temperature measured by Raman or emission spectroscopy. All spectra are Abel-inverted. First, the centerline spectra are presented. The results are shown in Figure 15.

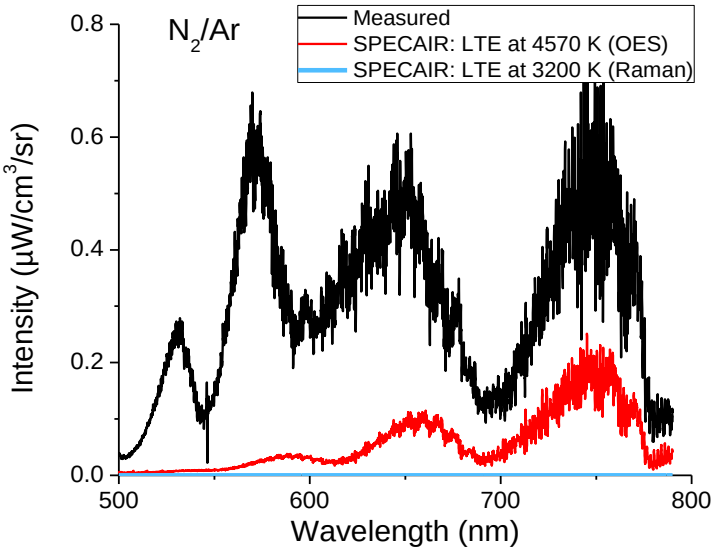

Figure 15: calibrated measured spectra and the corresponding computed spectra using SPECAIR, assuming equilibrium at the exit of the 15 cm tube. The measured spectra are Abel-inverted and only the emission of the 0.5 mm thick center slab is plotted.

There is again a clear discrepancy between the measured and the computed spectra assuming equilibrium at the temperatures measured with emission and Raman spectroscopy. The difference is significantly higher for the temperature measured with Raman spectroscopy. These results imply a nonequilibrium vibrational distribution within the N_2B state. As before, we altered the population of N_2B vibrational levels using overpopulations factor and the optimization algorithm. The final result, showing the experimental spectrum and the computed nonequilibrium spectrum, are in good agreement. Note that we assumed a Boltzmann distribution for the rotational levels of N_2B at the temperature measured with Raman spectroscopy. We also assumed that the rotational temperature is the same for each vibrational level. The influence of the rotational temperature on the results is discussed in Appendix A.

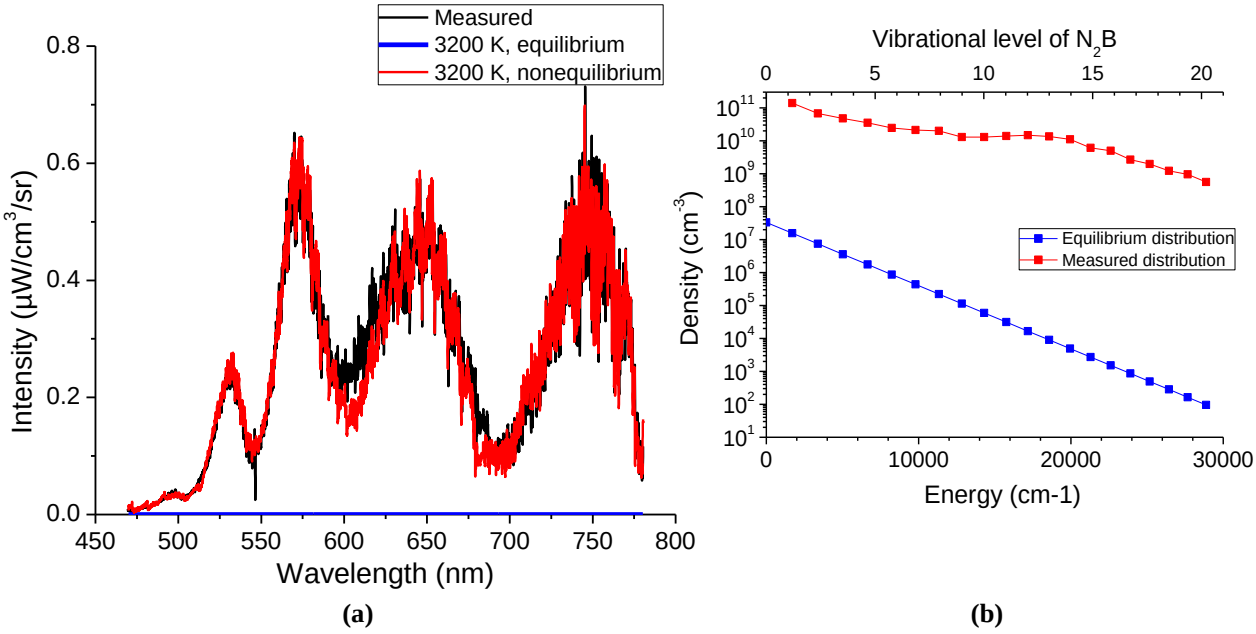

Figure 16: (a) Measured and computed spectra at the exit of the 15-cm tube for the N_2/Ar case at high mass flowrate. (b) Vibrational population distribution of N_2B taken for SPECAIR nonequilibrium calculations. To improve the fit, we added as a parameter of our optimization the overpopulation of N_2^+ (A $^2\Sigma_g^+$) corresponding to the transition N_2^+ Meinel.

The N_2B vibrational levels are highly overpopulated, much more than for the low mass flow rate N_2/Ar case. This is to be expected given that the higher gas velocity in the high mass flowrate case results in a reduction in the gas residence time in the tube, leaving less time for the recombining plasma to equilibrate. Furthermore, the increase in Reynolds number implies a turbulent flow which increases the heat transfer to the wall.

The overpopulation factors at several radial positions are shown in Figure 17. At each radial position, the vibrational levels of N_2B are overpopulated. Note that the absolute density of N_2B does not change significantly with the radial position despite the decrease of temperature with radial position. This leads to an increase of the overpopulation of N_2B.

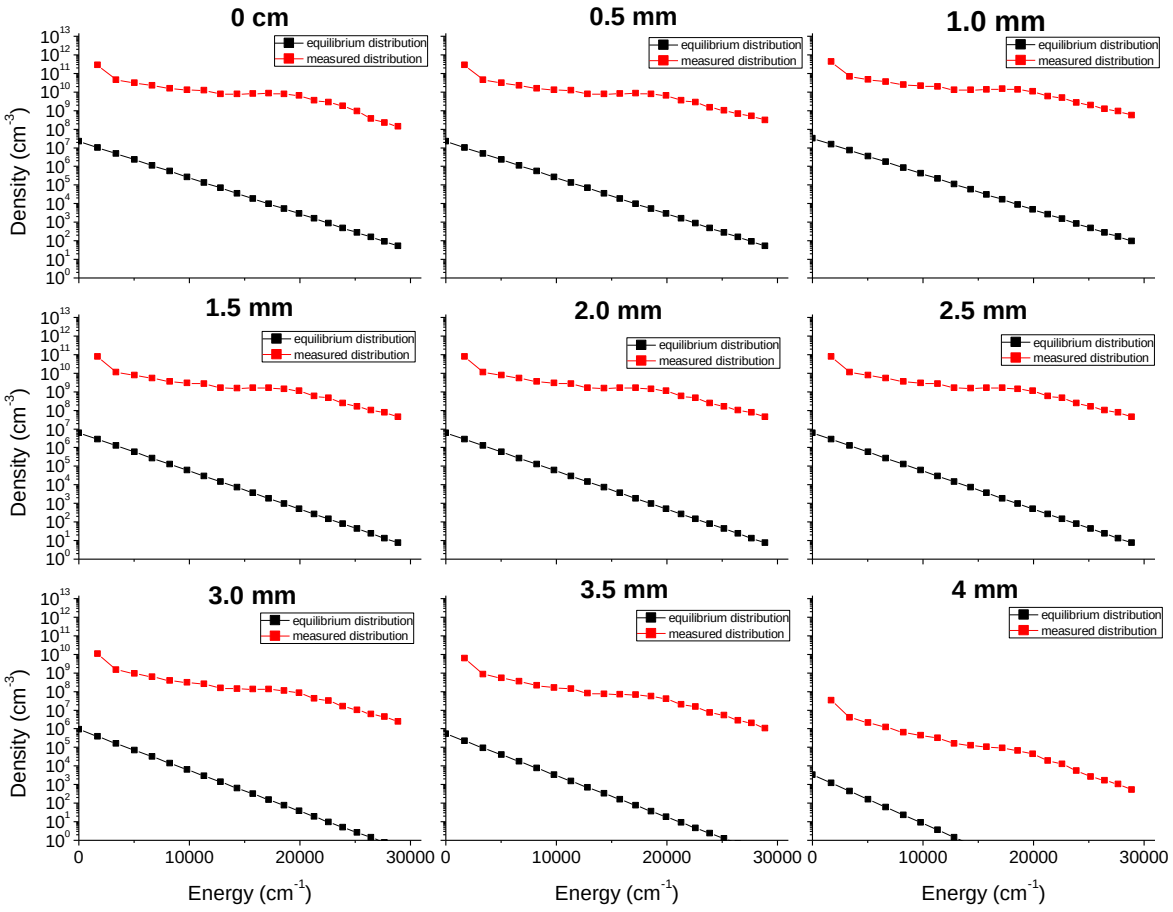

Figure 17: Population of vibrational levels of N_2B at different radial positions at the exit of a 15-cm tube exit. N_2/Ar plasma case at high flow rate.

The atomic N density was determined using the method presented in Section IIb. These measurements were performed at 10 and 15 cm. The results are presented in Figure 18.

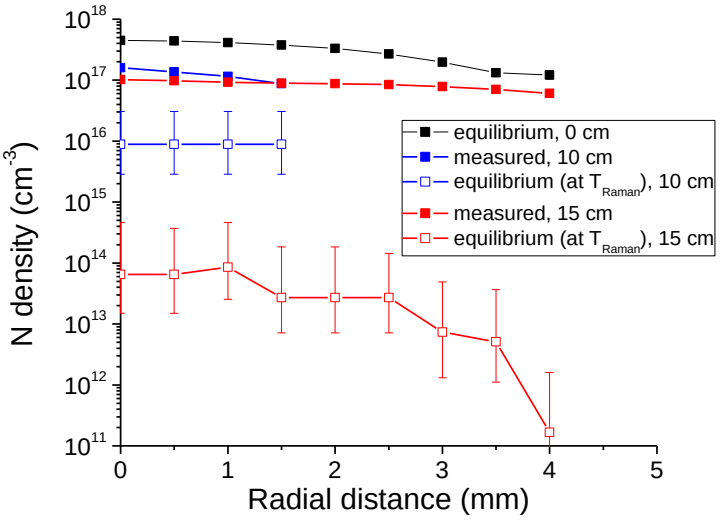

Figure 18: radial population distribution of atomic nitrogen at 0, 10 and 15 cm, measured and calculated assuming an equilibrium population at the temperature measured using Raman spectroscopy. N_2/Ar plasma case at high flow rate.

The density of atomic nitrogen is significantly above its equilibrium value at 10 cm and does not change substantially between 10 and 15 cm, suggesting that the population of N is not only frozen radially as discussed before, but also effectively frozen with axial distance beyond 10 cm. The atomic nitrogen density was also measured by Gessman *et al* at the center of the tube [18]. They measured a density of $(1.62\pm0.3) \cdot 10^{17}$ cm^3. This is to be compared with our measurement of $(1.02\pm0.06) \cdot 10^{17}$ cm^3.

A power balance analysis was performed using the same methodology as presented in Section IIb. The results are presented in Figure 19. The good agreement between the black and the blue curves suggests, as before, that the unrecombined N accounts for the missing power. Note that all the calculations were done using the temperature measured via Raman spectroscopy. The chemical power stored in the overpopulated vibrational levels of N_2 B (measured in Figure 16) and N_2 C, measured using emission spectroscopy, were also considered. Here again, this power is negligible in comparison with the power stored in the unrecombined N. This power balance gives us confidence in the fact that the temperature of the gas is indeed the temperature measured using Raman.

Although our measurements are self-consistent, they do not yield insight into the actual mechanism causing the rapid drop in temperature observed for all test cases: nitrogen/argon, air/argon and pure air plasmas. We examine this question with CFD models in the next section.

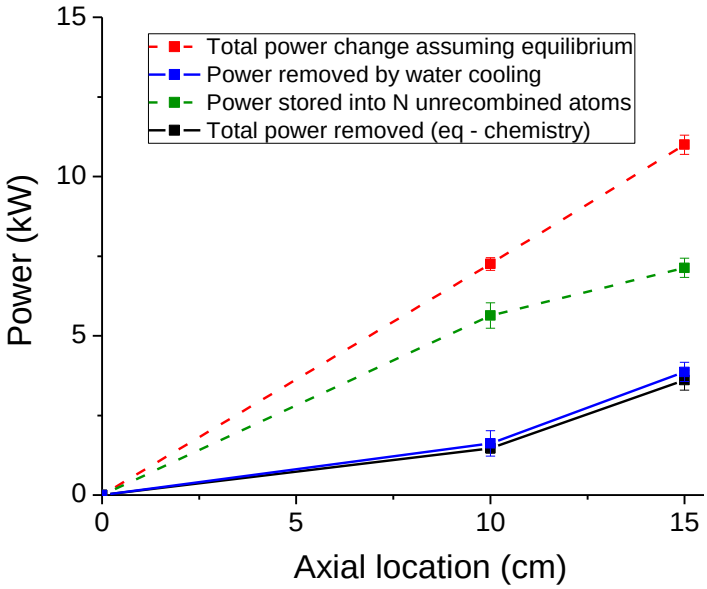

Figure 19: Power measurements using two approaches for the N_2/Ar plasma (high flowrate).

Discussion about N_2^+(B) rotational temperature

For both N_2/plasma cases, the temperature measured with OES at the exit of the 15-cm tube corresponds to the rotational temperature of N_2^+(B). This rotational temperature is higher than the temperature measured using Raman spectroscopy. Previous work suggested that, for recombining flows, the rotational temperature of N_2^+ may not be in equilibrium with the translational temperature [21]. Additional studies in shock tubes [22] [23] also showed that the vibrational and rotational temperatures of the N_2^+ first negative system could be significantly different from the gas temperature. These studies noted a similar trend in the N_2 second positive system. In addition, using the N_2^+ first negative system Venable *et al* [24] measured higher temperatures than the gas temperature. Devoto *et al* [25] noted a difference between the temperature using only the bandhead of the N_2^+ first negative system and that measured using all lines of this system. Both Venable and Devoto suggested that the population of high rotational levels of N_2^+(B) were not in equilibrium with the low lying rotational levels. Their assumptions were based on Griem's work [26] according to which such conditions can occur when the collisional-radiative relaxation time of a given state of an ion becomes lower than the thermalization time of electrons. This can occur for example when a steep gradient of temperature exists.

We have studied the reaction kinetics of N_2^+(B) in order to compare its production timescale with the R-T relaxation timescale. We will focus of the N_2/Ar plasma case presented in IIc) at the exit of a 15-cm tube. The R-T relaxation time can be obtained from Parker [27] and is approximately 8 ns at 3200K. Given that the plasma is in steady-state at the exit of the tube, the production time of N_2^+(B) is equal to its depletion time. The main reaction for removal of N_2^+(B) comes from collisional quenching with N_2 (Valk *et al* [28]):

R1: $$N_2^+(B) + N_2 \rightarrow N_2^+(X) + N_2$$

In our case, this gives a quenching time around 2 ns, which is smaller than the R-T rotational time. Therefore, N_2^+(B) is depleted before its rotational distribution can equilibrate with the gas temperature.

Given that the plasma is in steady-state at the exit of the water-cooled tube, the timescale for the production of N_2^+(B) must be equal to the timescale for the recombination N_2^+(B), i.e. about 2 ns. The mechanism for the fast production of N_2^+(B) is not understood at present. We review below several possible mechanisms, including direct production of N_2^+(B) or excitation of N_2^+(X) [29].

We first investigate the production of N_2^+(X). Three main reactions are considered, with reactions rates taken from the given references:

R2: $$N + N \rightarrow N_2^+(X) + e^-$$ [30] [31]

R3: $$N^+ + N_2 \rightarrow N_2^+(X) + N$$ [30] [31]

R4: $Ar^+ + N_2 \rightarrow N_2^+(X) + Ar$ [32] [33]

R5: $N_2(Y) + N_2(a') \rightarrow N_2(X) + N_2^+(X), \quad Y = A, a'$ [29] [34]

Only reaction R4 is fast enough (~2 ns) compared to the R-T relaxation time. Sonnenfroh *et al* [35] experimentally observed that the R4 reaction produced N_2^+ at rotational temperatures higher than that of the reactants. This could explain the high measured rotational temperature of N_2^+(B) if a fast reaction between N_2^+(B) and N_2^+(X) exists. This could occur via one of the following potential reactions:

R6: $N_2^+(X) + e^- \rightarrow N_2^+(B) + e^-$ [36]

R7: $N_2^+(X) + Ar^* \rightarrow N_2^+(B) + Ar$ [37]

R8: $N_2^+(X) + N_2(X, v \geq 12) \rightarrow N_2^+(B) + N_2(X, v - 12)$ [38]

The R7 rate was assumed to be similar to that excitation of N_2(X) by collisions with metastable argon atoms. R7 and R8 are the fastest reactions (~10 µs) but are still much slower than R-T relaxation. Note that high vibrational levels of N_2(X) can be populated via reactions with argon metastable atoms [39]. This could decrease the characteristic time of R8 by an order of magnitude.

N_2^+(B) can also be produced directly via:

R9: $N_2(X) + e^- \rightarrow N_2^+(B) + 2e^-$ [38]

R10: $N^+ + N + M \rightarrow N_2^+(B) + M$ [37]

R10 is the fastest method for the creation of N_2^+(B) (~1 µs) but is still slow compared to its recombination time and the R-T relaxation time.

Clearly, other reactions are probably at play to produce N_2^+(B) at time scales of less than 2 ns. These reactions are likely two-body reactions, but at present their rates are not known. Among possibilities, we could mention:

R11: $N_2^+(X, v > 12) + N_2 \rightarrow N_2^+(B) + N_2$

In conclusion, being under steady state conditions assures us than the rate of production of N_2^+(B) should be equal to its recombination rate. The time scale of this process, due to collisional quenching, is about 2 ns, which is smaller than the R-T relaxation time (~8 ns). It is therefore likely that N_2^+(B) is produced at high rotational temperature and does not have time to thermalize before it reacts. This would explain the higher measured rotational temperature of N_2^+(B) at the exit of a 15-cm tube for the b) and c) case.

II) CFD modeling of an equilibrium air

As seen in the previous sections, the recombining air mixture investigated was found to remain at or close to equilibrium. As a first step, we focus on modeling only an equilibrium case of a pure air plasma. This is the simplest to test CFD models.

The data for this test case is taken from Gessman et al [18]. For this case, the measured spectra corresponded well with spectra calculated assuming equilibrium conditions. The Reynolds number is about 1900 and the flow is therefore assumed laminar (Re < 2300).

The CFD simulations presented here were performed with the Eilmer3 code, a finite-volume Navier-Stokes flow solver [19] implemented on block-structured grids and developed at the Centre for Hypersonics at the University of Queensland. The computational domain corresponds to a 1-cm diameter tube that is 25 cm in length. The flow is assumed axisymmetric and a 2D simulation is performed. For the outlet boundary condition, the pressure is fixed at atmospheric pressure. As an alternate boundary condition at the tube exit, the presence of a reservoir was investigated but gave similar results. For the inlet boundary condition, the temperature profile is specified by extrapolating the measured temperature out to the wall diameter where the temperature is fixed at 300 K. The velocity profile is assumed to be self-similar to the temperature profile as mentioned before. The velocity profile is also constrained to satisfy the experimental mass flow rate. At the wall, we impose a boundary condition using ghost cells with a fixed temperature of 300 K along the tube wall. The heat flux is calculated using Fourier's law

between the ghost cell and the last cell in the plasma. The flow is laminar, and therefore no turbulence models are used. The gas is assumed to be at equilibrium everywhere in the tube, consistent with the conclusions of the measurements of Ref. [18]. The thermophysical properties (viscosity, thermal conductivity, density…) of the plasma are calculated using the NASA CEA code [20] to generate a database of the transport properties as a function of temperature. Comparisons between our simulations and the experiments of Gessman *et al* are presented in figure 20.

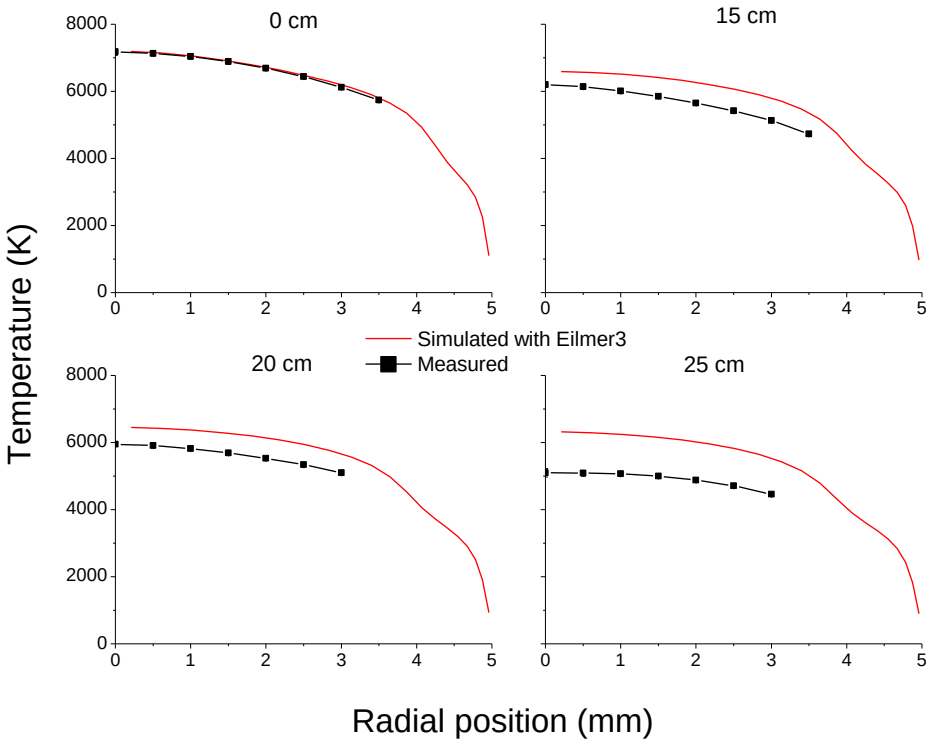

Figure 20: Comparison of measured and simulated (Eilmer3) temperature profiles at 0, 15, 20 and 25 cm for the pure air plasma.

For this laminar equilibrium case, Fig. 20 shows that the numerical predictions differ from the measurements. The slight change of the slope in the temperature profile near the wall is due to the presence of a local minimum in the equilibrium heat capacity around 4000 K calculated by CEA. This corresponds to the temperature interval in between oxygen and nitrogen dissociation. To examine the sensitivity of the predictions to the rate of heat transfer at the wall, we artificially increased the heat flux to the wall by a factor of 10, which is equivalent to multiplying the local thermal conductivity of the first cell (used in the Fourier's law) by 10. The temperature in the boundary cell close to the wall remains very close to the wall temperature. Thus, it appears that the cause for the discrepancy is an underprediction of radial heat transfer within the gas.

To confirm that assumption, we performed a parametric study on the thermal conductivity of the plasma. We added a conductivity varying exponentially with the temperature to model a possible radiative conductivity. The radiative conductivity of an air plasma may be estimated using the Rosseland approximation built in SPECAIR. The Rosseland approximation leads to the following radiative conductivity for a semitransparent medium:

$$\lambda_R(T) = \frac{4\pi}{3} n^2 \int_0^\infty \frac{1}{k_\lambda} \frac{d}{dT} L^\circ_\lambda(T) d\lambda$$

where n is index of refraction, L°_λ the radiance of the black-body from Planck's law, and k_λ is the spectral absorption coefficient [40]. It assumes that the plasma is optically thick. Note that, for our conditions, the plasma is not optically thick over all wavelengths. In the regions where the plasma is optically thin, k_λ is very small, which causes the conductivity integral to diverge. Therefore, a choice must be made regarding the range of wavelengths used in the integral. There are no well-defined and physically meaningful criteria for selecting this range and, furthermore, a small modification in this choice can have a large impact on the resulting conductivity. Thus the Rosseland conductivity is ill-defined here.

With these limitations in mind, we took as a starting reference point the radiative conductivity of an argon plasma reported in [41]. To obtain reasonable agreement between the Eilmer3 model and the measurements, the radiative conductivity must be 300 times higher than this reference value. The conductivities taken for this calculation are shown in figure 21 and the results in figure 22. Note that the equilibrium conductivity calculated using CEA corresponds to the sum of both the thermal and the reactive conductivities.

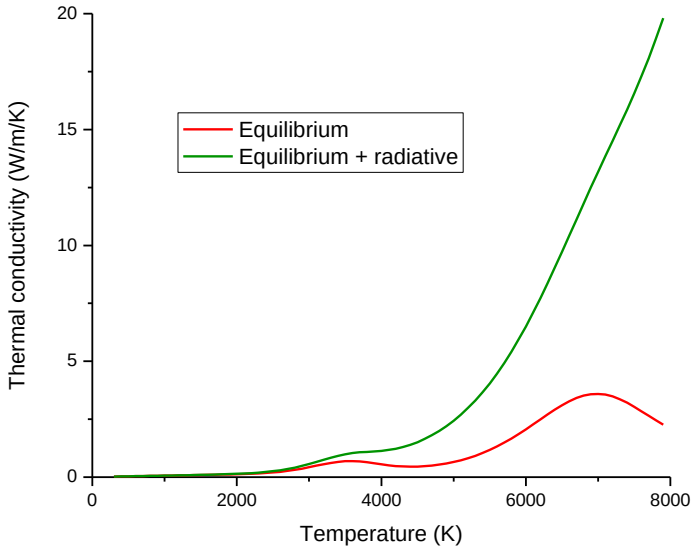

Figure 21: Thermal conductivity taken for our simulations as a function of the temperature

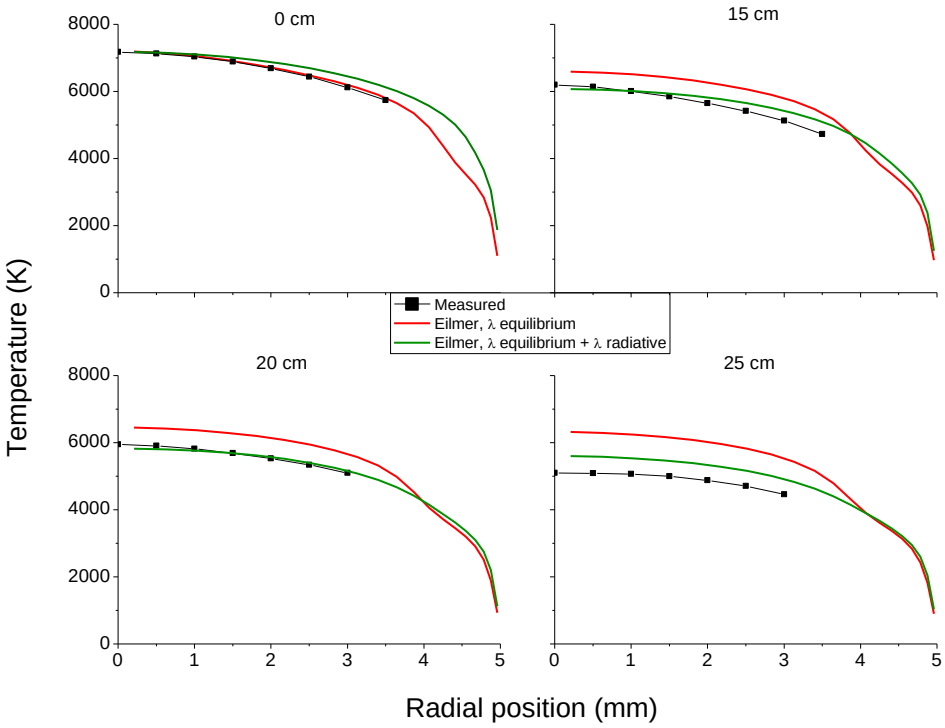

Figure 22: Comparison of the measured temperature profiles and those simulated with Eilmer3 for different thermal conductivities.

For both cases, the results between experiments and numerical simulations are in good agreement at 15 and 20 cm with the assumed radiative conductivity. Even so, there remains a discrepancy at 25 cm. This could come from effects due to turbulence. The Reynolds number of 1900 is estimated based on the conditions at 0 cm.

However, its value increases as the temperature decreases along the tube. At 25 cm, the Reynolds number is about 2600, which may indicate the presence of turbulence, and could help explain the observation that the drop in temperature between 20 and 25 cm is much higher than that between 15 cm and 20 cm.

Given the discrepancy between theoretical predictions and experimental measurements for this simple equilibrium case, a comparison with the more complexed nonequilibrium N_2/Ar test cases was not performed. Nevertheless, the results obtained for the pure air case suggest that radiation transport may play an important role. In future work, we intend to model this by coupling the fluid code with radiation transport.

III) Conclusions

Experiments have been conducted in a plasma torch facility to study equilibrium and nonequilibrium recombining plasmas of nitrogen/argon and air/argon mixtures. These experiments supply data that can be used to validate CFD and kinetic codes for recombining nitrogen and air plasmas. We have attempted to decouple this problem into two physical effects – hydrodynamic phenomena and chemical kinetic phenomena – by presenting data where the plasma remains in equilibrium and should be modeled using a comparatively simple hydrodynamic code, and cases where the plasma is strongly out of equilibrium and requires a detailed chemical kinetic model to be coupled to a fluid code.

We experimentally studied cases in chemical equilibrium (Air/Ar) and in chemical nonequilibrium (N_2/Ar). The Air/Ar plasma case served to validate our temperature measurements using Raman spectroscopy because these agreed with the emission spectroscopy measurements. For the case of an N_2/Ar plasma, the Raman measurements yielded a much lower temperature than the emission spectroscopy measurements. Similar phenomena were observed by other authors [42] and potential explanations were given. Furthermore, strong evidence of chemical nonequilibrium was found in the emission spectroscopy measurements. Both N_2/Ar cases gave similar results although the high flow rate case was farther out of equilibrium than the low mass flow rate case.

Based on the temperature measured using Raman spectroscopy, we were able to calculate overpopulation factors for the N_2B state in order to describe the observed nonequilibrium. The absolute density of atomic N was also inferred from the first positive emission of N_2. Finally, a simple energy balance showed that a large portion of enthalpy remains in the unrecombined atomic nitrogen. This case is therefore useful to test QSS kinetic models such as that previously implemented in Ref. [7].

The CFD model Eilmer3 was used to simulate the temperature drop for an equilibrium case. This fluid code underpredicts the measured temperature drop in the tube. For this case, the discrepancy between CFD and experiments cannot be explained by chemical kinetics as the plasma remains in equilibrium. Given our CFD predictions and experimental results, it appears that the reason for the discrepancy is due to an inability to model the radial heat transfer within the gas.

These recombining plasmas raise many interesting issues for the CFD community to resolve. The experiments were done using a simple configuration and, therefore, present a relatively seemingly simple test case for the modeling of nonequilibrium recombining air and nitrogen flows. Yet, as shown in the paper, challenges remain to correctly simulate these test cases. These issues are currently the object of our continued investigations.

Acknowledgments

This work has been supported by Ariane Group, under a CIFRE Ph.D. grant (number 42701092/20160218/JSE), with Dr. Laurent Visconti as Technical Monitor. We would like to thank Professors Peter Jacobs and Rowan Gollan (University of Queensland) for their help with the Eilmer3 code.

Appendix A: Influence of rotational temperature of N_2B on the computed spectra

For N_2/Ar plasmas, in figures 12 and 18, we plotted the computed spectrum using SPECAIR assuming a nonequilibrium vibrational distribution. The rotational temperature was assumed to be equal to the temperature measured using Raman spectroscopy. However, recall that emission measurements of the rotational temperature of N_2^+ B were higher than the Raman temperature. Given this, it is not clear what rotational temperature to use for the simulation of the first positive emission of N_2. This issue will be discussed in this appendix.

For this analysis, we focus on the N_2/Ar plasma test case presented in section IIc (high flow rate). The measured spectrum was not sufficiently resolved in wavelength to directly measure the rotational lines of N_2B and infer a rotational temperature. Thus we conducted a parametric study on the N_2B rotational temperature. In our optimization algorithm, we then altered the population of the N_2B vibrational levels. Because the final distribution is not Boltzmann, the measured population of any given vibrational state was defined relative to its equilibrium value at the chosen rotational temperature. This was done through the use of the overpopulation factor. In the results presented in section II, the rotational temperature was fixed to the temperature measured using Raman spectroscopy as this was felt to be more representative of the bulk gas temperature. We will now change the rotational from 2500 K to 5500 K and, for each temperature, determine the corresponding overpopulation factors. Note that we assume that all vibrational levels of N_2B have the same rotational temperature in this study because the measured spectrum is not sufficiently resolved in wavelength to have an accurate result and it will add many degrees of freedom to the fitting algorithm. We compare the total relative error between the measured spectrum and the one resulting from our algorithm for each rotational temperature. Figure A.1 shows the relative error between spectra for this calculation.

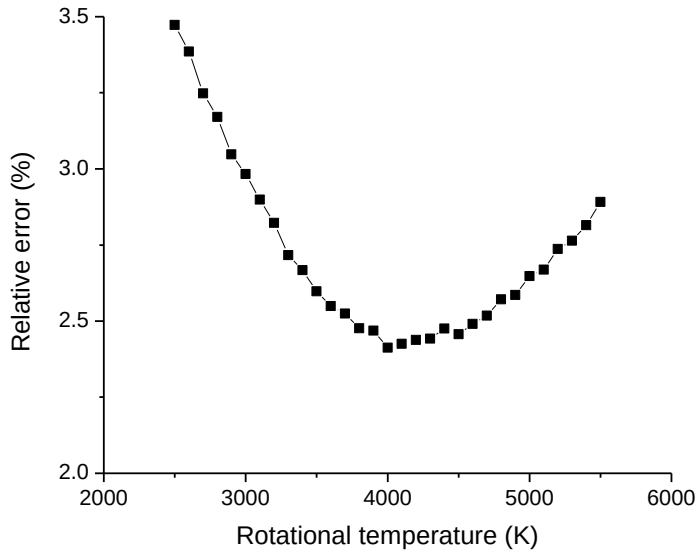

Figure A.1: Relative error between measured spectrum and computed one using SPECAIR assuming a nonequilibrium vibrational population of N_2B for several rotational temperatures.

Note the presence of a local minimum around 4000 K. This may indicate that the rotational temperature of N_2B is closer to this temperature. We have also plotted on figure A.2 the resulting spectrum from our algorithm for several rotational temperatures, as well as the experimental spectrum.

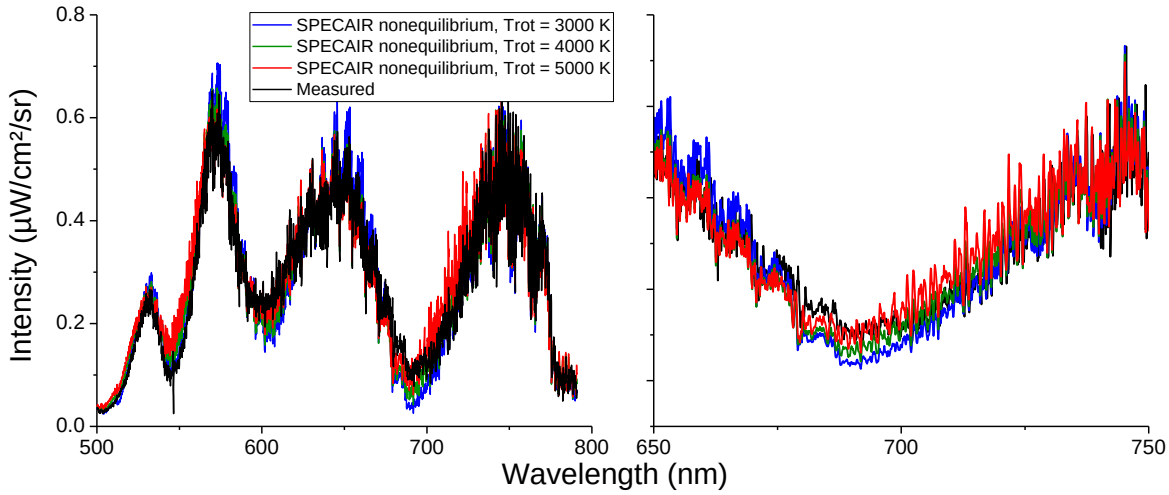

Figure A.2: Measured spectrum and computed one using SPECAIR assuming a nonequilibrium vibrational population of N_2B for several rotational temperatures. Left: spectrum from 500 nm and 800 nm. Right: zoom on region between 650 and 750 nm

Note that the temperature of 4000 K gives a better agreement with experiments, particularly in the region where the emission is lower. Beyond this analysis, we have no justification for fixing the rotational temperature to 4000 K. It was for this reason that the Raman temperature measurement was used for the analysis. Additional measurements are necessary to resolve this problem: high resolution measurements of the first positive system would be very valuable to that end. We can still note that based on this analysis, the rotational temperature of N_2B is likely to be higher than the temperature measured with Raman spectroscopy, as is the rotational temperature of N_2^+B measured with emission spectroscopy.

As a final note, figure A.3 shows the absolute population of the vibrational levels of N_2B resulting from our algorithm for various rotational temperature inputs. As expected, the absolute population of the vibrational levels of N_2B is not significantly dependent of the rotational temperature.

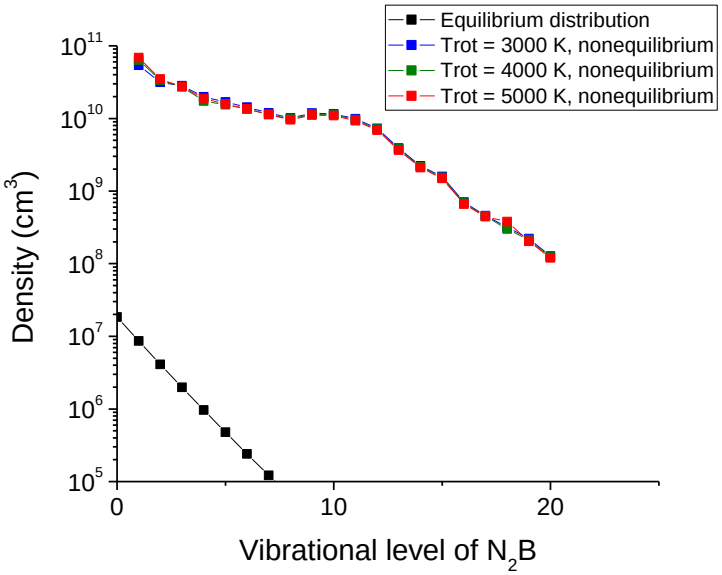

Figure A.3: Population of vibrational levels of N_2B with optimization algorithm at several rotational temperatures

References:

[1] P. A. Gnoffo, «Planetary-Entry Gas Dynamics,» *Annual Review of Fluid Mechanics,* vol 31, pp. 459-494, 1999.

[2] C. O. Johnston, P. A. Gnoffo et A. Mazaheri, «Influence of Coupled Radiation and Ablation on the Aerothermodynamic Environment of Planetary Entry Vehicles,» *Radiation and Gas-Surface Interaction Phenomena in High Speed Re-Entry; 6-8 May 2013*

[3] S. Loehle, T. A. Hermann, F. Zander, H. Fulge et T. Marynomwski, «Ablation Radiation Coupling Investigation in Earth Re-entry Using Plasma Wind Tunnel Experiments,» *American Institute of Aeronautics and Astronautics, AIAA 2014-2250,* 2014.

[4] M. E. MacDonald, C. M. Jacobs, C. O. Laux, F. Zander et R. G. Morgan, «Measurements of air plasma/ablator interactions in an inductively coupled plasma torch,» *J. Thermophys. Heat Transfer,* vol. 29, pp. 12-23, 2015.

[5] S. D. McGuire, A. C. Tibère-Inglesse et C. O. Laux, «Infrared spectroscopic measurements of carbon monoxide within a high temperature ablative boundary layer,» *Journal of Physics D: Applied Physics,* vol. 49, n°48, 2016.

[6] C. O. Laux, R. J. Gessmann et C. H. Kruger, «Ionizational Nonequilibrium Induced by Neutral Chemistry in Air Plasmas,» *AIAA journal,* vol. 34, n° 8, pp. 1745-1747, Aug 1996.

[7] C. O. Laux, L. Pierrot et R. J. Gessman, «State-to-state modeling of a recombining nitrogen plasma experiment,» *Chemical Physics,* vol. 398, pp. 46-55, 2012.

[8] G. V. Candler, C. O. Laux, R. J. Gessman et C. H. Kruger, «Numerical Simulation of a Nonequilibrium Nitrogen Plasma Experiment,» *28th Plasmadynamics and Lasers Conference, Fluid Dynamics and Co-located Conferences,* AIAA 1998-2365, 1997.

[9] M. Nagulapally, D. Kolman, G. V. Candler, C. O. Laux, R. J. Gessman et C. H. Kruger, «Numerical Simulation of Nonequilibrium Nitrogen and Air Plasma Experiments,» *29th AIAA, Plasmadynamics and Lasers Conference, Fluid Dynamics and Co-located Conferences,* AIAA 1998-2665 , 1998.

[10] C. O. Johnston and A. M. Brandis, "Features of Afterbody Radiative Heating for Earth Entry," *Journal of Spacecraft and Rockets, Vol. 52,* vol. 52, pp. 105-119, 2015.

[11] C. O. Johnston, A. M. Brandis et K. Sutton, «Shock Layer Radiation Modeling and Uncertainty for Mars entry,» *43rd AIAA Thermophysics Conference, Fluid Dynamics and Co-located Conferences,* AIAA 2012-2866, 2012.

[12] R. J. Gessman, C. O. Laux et C. H. Kruger, «Experimental study of kinetic mechanisms of recombining atmospheric pressure air plasmas,» *28th AIAA Plasmadynamics and Lasers Conference,* AIAA 97-2364, 1997.

[13] C. O. Laux, «Optical diagnostics and radiative emission of air plasmas,» *PhD Thesis, Stanford University,* 1993.

[14] C. O. Laux, R. J. Gessman, C. H. Kruger et S. P. Davis, «Rotational temperature measurements in air and nitrogen plasmas using the first negative system of N_2^+,» *Journal of Quantitative Spectroscopy and Radiative Transfer,* vol. 68, pp. 473-482, 2001.

[15] SPECAIR, Software Package, Ver. 3.0,, Spectral Fit S.A.S., www.spectralfit.com.

[16] C. O. Laux, T. G. Spence, C. H. Kruger et R. N. Zare, «Optical diagnostics of atmospheric pressure air plasmas,» *Plasma Sources Science and Technology,* vol. 12, n° 2, 2003.

[17] S. D. McGuire, A. C. Tibère-Inglesse et C. O. Laux, «Ultraviolet Raman spectroscopy of N_2 in a recombining atmospheric pressure plasma,» *Plasma Sources Science and Technology,* vol 26, n° 11, 2017.

[18] R. J. Gessman, «An experimental investigation of the effects of chemical ionizational nonequilibrium in recombining atmospheric pressure air plasmas,» *PhD thesis, Stanford University, 2000.*

[19] R. J. Gollan et P. A. Jacobs, «About the formulation, verification and validation of the hypersonic flow solver Eilmer,» *International Journal for Numerical Methods in Fluids,* vol. 73, n°1, pp. 19-57, 2013.

[20] B. J. McBride et S. Gordon, «Computer Program for Calculation of Complex Chemical Equilibrium Compositions and Applications II. User's Manual and Program Description,» *NASA RP-1311-P2,* 1996.

[21] D. Studer et P. Vervisch, «Raman scattering,measurements within a flat plate boundary layer in an,inductively coupled plasma wind tunnel,» *Journal of Applied Physics,* vol. 102, n° 3, 2007.

[22] K. Fujita, S. Sato et T. Abe, «Experimental Investigation of Air Radiation from Behind a Strong Shock Wave,» *Journal of Thermophysics and Heat Transfer,* vol. 16, n° 1, p. 77-82, 2002.

[23] S. P. Sharma, «Vibrational and rotational temperature measurements in a shock tube,» *Proceedings of the Eighteenth International Symposium on Shock Waves,* vol. 1, pp. 683-690, 1992.

[24] W. Venable, «Observations of departures from equilibrium in a nitrogen arc,» *Journal of Quantitative Spectroscopy and Radiative Transfer,* vol. 9, pp. 1215-1226, 1969.

[25] R. S. Devoto, U. H. Bauder, J. Cailleteau et E. Shires, «Air transport coefficients from electric arc measurements,» *The*

Physics of Fluids, vol. 21, n° 4, pp. 552-558, 1978.

[26] H. R. Griem, Principles of Plasma Spectroscopy, Cambridge University Press, 2005.

[27] J. G. Parker, «Rotational and Vibrational Relaxation in Diatomic Gases,» *The Physics of Fluids*, vol. 2, n° 4, pp. 449-462, 1959.

[28] F. Valk, M. Aints, P. Paris, T. Plank, J. Maksimov et A. Tamm, «Measurement of collisional quenching rate of nitrogen states $N_2(C\ ^3\Pi_u, v = 0)$ and N_2^+ $(B\ ^2\Sigma_g^+, v=0)$,» *Journal of Physics D: Applied Physics*, 2010.

[29] V. Linss, H. Kupfer, S. Peter et F. Richter, «Two N_2^+ $(B\ ^2\Sigma_u^+)$ populations with different Boltzmann distribution of the rotational levels found in different types of N_2/Ar discharges—improved estimation of the neutral gas temperature,» *Journal of Physics D: Applied Physics*,, vol. 37, n° 14, 2004.

[30] C. Park, «Review of chemical-kinetic problems of future NASA missions. I - Earth entries,» *Journal of Thermophysics and Heat Transfer*, vol. 7, n° 3, pp. 385-398, 1993.

[31] R. N. Gupta, J. M. Yos, R. A. Thompson et K.-P. Lee, «A Review of Reaction Rates and Thermodynamic and Transport Properties for an 11-Species Air Model for Chemical and Thermal Nonequilibrium Calculations to 30 000 K,» *NASA technical report, NASA-RP-1232*, 1990.

[32] R. C. Amme et H. C. Hayden, «Ion-Beam Excitation Effects on the Single Charge Transfer between Argon and Nitrogen,» *The Journal of Chemical Physics*, vol. 42, 1965.

[33] A. A. Viggiano, J. M. Van Doren, R. A. Morris et J. F. Paulson, «Evidence for an influence of rotational energy on the rate constants for the reaction of $Ar^+(^2P_{3/2})$ with N_2,» *The Journal of Chemical Physics* , vol. 93, n° 7, p. 4761-4765, 1990.

[34] H. Brunet, P. Vincent et J. Rocca Serra, «Ionization mechanism in a nitrogen glow discharge,» *Journal of Applied Physics*, vol. 54, n° 9, p. 4951-4957, 1983.

[35] D. M. Sonnenfroh et S. R. Leone, «A laser-induced fluorescence study of product rotational state distributions in the charge transfer reaction: $Ar^+(^2P_{3/2}) + N_2 \rightarrow Ar + N_2^+(X)$ at 0.28 and 0.40 eV,» *The Journal of Chemical Physics*, vol. 90, n° 3, p. 1677-1685, 1989.

[36] D. H. Crandall, W. E. Kauppila, R. A. Phaneuf, P. O. Taylor et G. H. Dunn, «Absolute cross sections for electron-impact excitation of N_2^+,» *Physical Review A*, vol. 9, pp. 2545-2551, 1974.

[37] M. N. Shneider, A. Baltuška et A. M. Zheltikov, «Population inversion of molecular nitrogen in an Ar: N_2 mixture by selective resonance-enhanced multiphoton ionization,» *Journal of Applied Physics*, vol. 110, n° 8, 2011.

[38] B. Massabieux, A. Plain, A. Ricard, M. Capitelli et C. Gorse, «Excitation of vibrational and electronic states in a glow discharge column in flowing N_2,» *Journal of Physics B: Atomic and Molecular Physics*, vol. 16, n° 10, 1983.

[39] M. Touzeau et D. Pagnon, «Vibrational excitation of $N_2(C)$ and $N_2(B)$ by metastable argon atoms and the determination of the branching ratio,» *Chemical Physics Letters*, vol. 15, pp. 355-360, 1978.

[40] J. Taine, E. Iacona et J.-P. Petit, Transferts thermiques: Introduction aux transferts thermiques, Dunod, 2008.

[41] T. G. Owano, C. H. Kruger et R. A. Beddini, «Electron-ion three-body recombination coefficient of argon,» *AIAA Journal*, vol. 31, n° 1, pp. 75-82, 1993.

[42] P. J. Bruggeman, N. Sadeghi, D. C. Schram et V. Linss, «Gas temperature determination from rotational lines in nonequilibrium plasmas: a review,» *Plasma Sources Science and Technology*, vol. 23, 2014.